Nanocomposite of Tin Sulfide Nanoparticles with Reduced Graphene Oxide in High-Efficiency Dye-Sensitized Solar Cells

Bo Yang,[†] Xueqin Zuo,[†] Peng Chen,[†] Lei Zhou,[†] Xiao Yang,[†] Haijun Zhang,[†] Guang Li,*,[†,‡] Mingzai Wu,[†,‡] Yongqing Ma,[†,‡] Shaowei Jin,[†,‡] and Xiaoshuang Chen[§]

[†]School of Physics and Materials Scienceand [‡]Anhui Key Laboratory of Information Materials and Devices, Anhui University, Hefei 230601, China

[§]National Laboratory for Infrared Physics, Shanghai Institute of Technical Physics, Chinese Academy of Sciences, Shanghai 200083, China

S *Supporting Information*

ABSTRACT: A nanocomposite of SnS_2 nanoparticles with reduced graphene oxide (SnS_2@RGO) had been successfully synthesized as a substitute conventional Pt counter electrode (CE) in a dye-sensitized solar cell (DSSC) system. The SnS_2 nanoparticles were uniformly dispersed onto graphene sheets, which formed a nanosized composite system. The effectiveness of this nanocomposite exhibited remarkable electrocatalytic properties upon reducing the triiodide, owning to synergistic effects of SnS_2 nanoparticles dispersed on graphene sheet and improved conductivity. Consequently, the DSSC equipped with SnS_2@RGO nanocomposite CE achieved power conversion efficiency (PCE) of 7.12%, which was higher than those of SnS_2 nanoparticles (5.58%) or graphene sheet alone (3.73%) as CEs and also comparable to the value (6.79%) obtained with pure Pt CE as a reference.

KEYWORDS: SnS_2@RGO, nanocomposites, counter electrode, DSSC
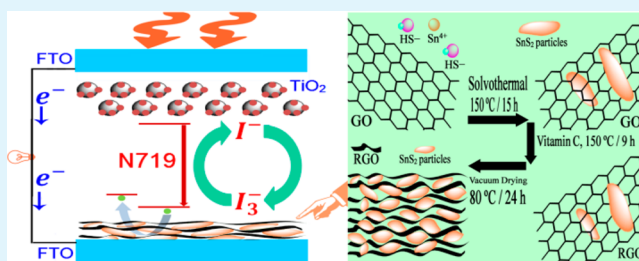
1. INTRODUCTION

Since the inception of the new century, energy situations have undergone severe challenges. People are looking for some renewable energy sources. As a future energy source, solar energy is endowed with high expectations.[1] Dye-sensitized solar cells (DSSCs) have attracted tremendous interest and large-scale research in numerous academic laboratories because of their high efficiency, simple fabrication process, pollution-free nature, and low consumption.[2] A typical DSSC structure included transparent conducting optical glass, photoanode, dyes, electrolyte, and counter electrode (CE).[3,4] As a crucial component, an ideal CE for DSSC should possess high conductivity and superior catalytic properties. After a decade of development, the types of CE materials are particularly abundant, including noble metals (such as Pt), carbon materials, metal oxides, and sulfides.[5−8] Furthermore, composites (supported catalysts) are widely used for CEs.[9,10]

Composite materials are composed of two or more kinds of materials joined by physical or chemical methods, which can exhibit new performance characteristics.[11] Graphene is a new member of the carbon crystal family that has a unique one-atom-thick two-dimensional layer of sp^2-bonded crystal structure and has a variety of excellent properties such as high carrier mobility, electric conductivity, thermal conductivity, and transparency.[12] It also has been used as a CE in DSSCs.[13] SnS_2 is a crucial mid-band-gap (E_g = 2.2 eV)

semiconductor,[14] whose high electrical conductivity and appealing catalytic activity has been demonstrated in lithium batteries and DSSCs.[6,15,16] However, neither pure reduced graphene oxide (RGO) nor bare SnS_2 can achieve excellent conversion efficiency as a CE in DSSCs. To solve this disadvantage, a composite of SnS_2 with RGO may be a great choice. This material has been applied in lithium battery as a perfect strategy to improve the performance.[17,18] Particularly worth mentioning is that we have successfully loaded Bi_2S_3 onto graphene in our previous work and achieved power conversion efficiency (PCE) of 5.5%, nearly triple the best conversion efficiency value of the DSSC with Bi_2S_3 but without graphene.[19]

In this paper, we focus our investigations on the synthesis of SnS_2@RGO nanocomposite by a modification of the two-step strategy we have used for compounding Bi_2S_3/graphene nanocomposite.[19,20] Fortunately, SnS_2 was uniformly dispersed on the graphene sheet. Meanwhile, our main attention was centered on exploring a synergy mechanism of SnS_2 on graphene and studying its catalytic ability used as the counter electrode of a DSSC. This is the first time that we have used SnS_2@RGO nanocomposite for application as CE in DSSC. On

account of the introduction of RGO into system, our materials achieve a PCE value of 7.12%, which is comparable to the 6.79% obtained with pure Pt CE as a reference.

2. EXPERIMENTAL SECTION

All reagents were of analytical grade and were purchased and used as received without further purification.

2.1. Synthesis of Graphene Oxide. Graphene oxide (GO) nanosheets were prepared by a modified Hummers method.[21] In detail, concentrated H_2SO_4 and concentrated H_3PO_4 were mixed in a 500 mL beaker, followed by addition of graphite powder. The beaker was put in a preheated 50 °C water bath with magnetic stirring, followed by slow addition of $KMnO_4$ to ensure that the temperature was maintained at about 50 °C. After the addition of $KMnO_4$, stirring was continued for another 6 h at 50 °C. Then diluted H_2O_2 was added into the solution without interruption until no bubbles were produced, while the color of the solution changed from black to purple and finally became bright yellow. The mixture was stirred for another 3 h. The final solid product was cooled to room temperature and separated by centrifugal separation, and then washed with HCl (5%), alcohol, and deionized water in turn until the supernatant was close to neutral, and graphene oxide was obtained. The collected sediment was dispersed in alcohol and was followed by an ultrasonic treatment. Subsequently, the concentration of the graphene oxide suspension solution was calculated by weighing the mass of the sample after drying at 90 °C for 24 h. Reduced graphene oxide was prepared by a solvothermal method with L-ascorbic acid as reductant.

2.2. Preparation of SnS_2@RGO Nanocomposite and Pure SnS_2 Nanoparticles. Synthesis of SnS_2@RGO is shown in Scheme 1.

Scheme 1. Illustration of Synthesis of SnS_2@RGO Nanocomposites
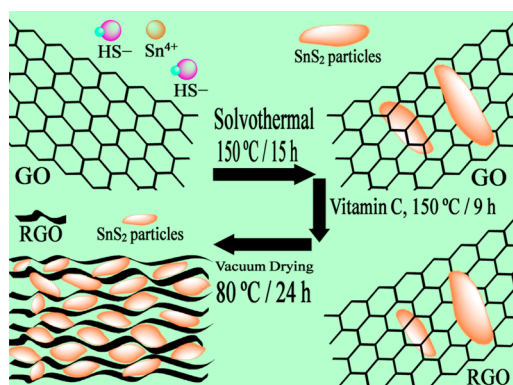
GO was selected as the raw material for this work. The concentration of the final GO alcohol suspension was 1.3 mg/mL. A two-step method to synthesize the compound was utilized for this process. In the first step, 80 mL of GO alcohol suspension was added into a 250 mL beaker, 2.5 mmol of $SnCl_4\cdot5H_2O$ was added with magnetic stirred to form a uniform solution, and then 5 mmol of L-cysteine hydrochloride monohydrate was added. Then the compound was transferred into the autoclave for solvothermal treatment at 150 °C for 15 h. In the second step, after the autoclave was cooled to room temperature, 3 mmol of L-ascorbic acid was added to the mixture, which was stirred with a magnetic stirrer. The mixture was then sealed into an autoclave for reaction at 150 °C for 9 h. The final sediment was washed with alcohol and deionized water and separated by centrifugation,[19] and then the SnS_2@RGO hybrid was obtained. Pure SnS_2 nanoparticles were obtained under the same reaction conditions.

2.3. Characterization. The as-synthesized samples were characterized by X-ray powder diffraction (XRD) with monochromatized Cu Kα radiation (λ = 1.5406 Å) at 36 kV and 25 mA. Transmission electron microscopy (TEM) images were acquired on a JEOL JEM-100SX transmission electron microscope at an acceleration voltage of 200 kV. Raman spectroscopy was performed on a Renishaw Via-Reflex Raman spectrometer with a laser of 532 nm. Fourier transform infrared spectroscopy (FT-IR) was carried on a American Nicolet Instrument Co. Nexus-870 FT-IR instrument with wavelength range from 2000 to 100 cm^{-1}. UV−vis spectra were acquired on a liquid Hitachi U-4100 spectrophotometer. All measurements were performed at room temperature.

2.4. Fabrication of Counter Electrodes. CEs were typically prepared by dispersing SnS_2@RGO (SnS_2@RGO, SnS_2, and RGO powders were used as raw material to prepare CEs, respectively) powder (0.12 g) and poly(ethylene glycol) powder (0.04 g) in 1 mL of absolute ethanol and then grinding with a mortar to form a gelatin. Subsequently, the gelatin was coated on fluorine-doped tin oxide (FTO) conductive glass followed by natural drying and annealing at 400 °C (the optimal annealing temperature; see Figure S1 in Supporting Information) for 60 min under the protection of argon. After natural cooling to room temperature, the CEs were formed. Figure S3 (Supporting Information) shows the SEM image of SnS_2@RGO nanocomposites CE.

2.5. Assembly of Dye-Sensitive Solar Cells. A DSSC device was combined by sandwiching electrolyte between a dye-sensitized TiO_2 anode and an as-prepared FTO-supported SnS_2@RGO (CEs were prepared by dispersing SnS_2@RGO, SnS_2, and RGO nanoparticle, respectively) nanoparticle CE. The purchased TiO_2 anode, whose colloid film had a thickness of 10 μm and area of 0.25 cm^2, was sensitized by steeping in a 0.50 mM ethanol solution of N719 dye for 24 h. The electrolyte consisted of 0.1 M LiI, 0.12 M I_2, 1.0 M 1,2-dimethyl-3-propylimidazolium iodide (DMPII), 0.5 M of 4-tert-buylpyridine, and 10 mL of 3-methylpropionitrile.[22]

2.6. Electrochemical Characterization. Electrochemical performance was tested by use of a Zennium electrochemical analyzer workstation (Zahner Co.), which was composed of an Ag/AgCl reference electrode, a working electrode of FTO glass-supported SnS_2 and a CE of platinum sheet. Cyclic voltammetry (CV) curves were recorded in a supporting electrolyte consisting of 10 mM LiI, 1 mM I_2, and 100 mM $LiClO_4$ in acetonitrile at a scan rate of 50 mV·s^{-1}. Electrochemical impedance spectroscopy (EIS) measurements were recorded in a frequency range of 0.01∼10^6 kHz and at alternating current amplitude of 10 mV. Tafel polarization curves were recorded by assembling symmetric cells fabricated with FTO/SnS_2@RGO, redox electrolyte, and FTO/SnS_2@RGO, and the test of pure SnS_2 and RGO were assembled into the same device, respectively.

2.7. Photovoltaic Measurements. Photocurrent density−voltage (J−V) curves were recorded by use of a xenon lamp solar simulator under AM 1.5 illumination and gauged under 100 mW·cm^{-2}, which was calibrated beforehand by an optical power meter.

3. RESULTS AND DISCUSSION

Figure 1 shows the XRD patterns of SnS_2@RGO, SnS_2, GO, and RGO samples. GO presented a typical peak at 10.5°, which corresponds to an interplanar spacing of 0.84 nm.[10] Upon reduction of GO via a solvothermal method with L-(+)-ascorbic acid,[19] the typical peak shifted to 25.8° and became broadened, which corresponds to the characteristic peak of graphene.[10] Meanwhile, all the XRD peaks of as-synthesized SnS_2 sample could be well indexed by referring to JCPDS 23-0677. No characteristic peaks were observed for other impurities such as S, SnS, and SnO_2. This indicated that pure SnS_2 was prepared. The nanocomposites also showed diffraction peaks for SnS_2 and a slight signal for RGO at nearly 26°. Here we put forward a speculation: when the nanocomposites were prepared, SnS_2 nanoparticles were attached to the RGO layer during the reaction process. Hence, we could speculate that the SnS_2 nanoparticles aggregate and restack onto the RGO sheet. This speculation could be evidenced by further demonstrations in the following discussion.
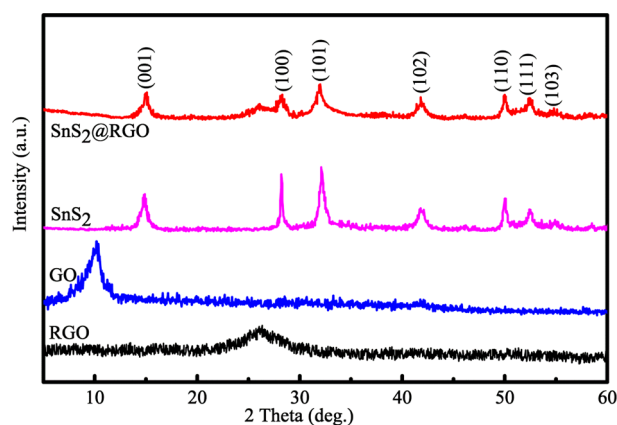
Figure 1. XRD patterns of SnS$_2$@RGO, SnS$_2$, GO, and RGO.

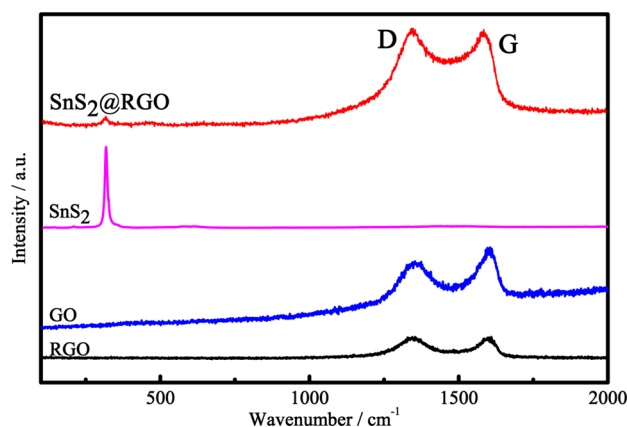The Raman spectra of as-prepared SnS$_2$@RGO, SnS$_2$, GO, and RGO are given in Figure 2. Two characteristic peaks in

Figure 2. Raman spectra of SnS$_2$@RGO, SnS$_2$, GO, and RGO.

accordance with the D and G bands of GO (at 1352 and 1601 cm^{-1}, respectively) were clearly observed. The D band is the structure defect of graphene, while the G band belongs to the E$_{2g}$ phonon of C sp^2 atoms.[23,24] The Raman spectrum of RGO also comprised both D and G bands (at 1352 and 1596 cm^{-1}, respectively). Interestingly, the D band did not change when GO was reduced to RGO, demonstrating that the number of layers was unchanged.[25] For GO, the intensity ratio of D band to G band (I_D/I_G) was 0.843, which increased to 1.017 for RGO, corroborating the reduction of GO.[26] The I_D/I_G ratio of SnS$_2$@RGO was 1.005, very close to that of RGO. This suggested that SnS$_2$ nanoparticles were absorbed into RGO layers, not doped onto graphene. The Raman spectrum of pure SnS$_2$ showed a stretching vibration peak at 311 cm^{-1} relative to the A$_{1g}$ mode of SnS$_2$, and this evidenced the formation of SnS$_2$@RGO nanocomposite.[17] On the basis of the analysis above, we could confirm that our previous speculation was correct: the graphene-based SnS$_2$ sandwich nanocomposite was successfully prepared.

The FT-IR spectra of SnS$_2$@RGO and GO are shown in Figure 3. In GO, a strong and broad absorption at 3408 cm^{-1} was observed, which was due to O−H stretching vibration. We observed the C=O stretching of -COOH groups located at the edges of GO sheets at 1735 cm^{-1}. As a result of the O−H bending vibration, skeletal ring vibrations, and epoxide groups, absorptions were observed around 1624 cm^{-1}. The spectrum of
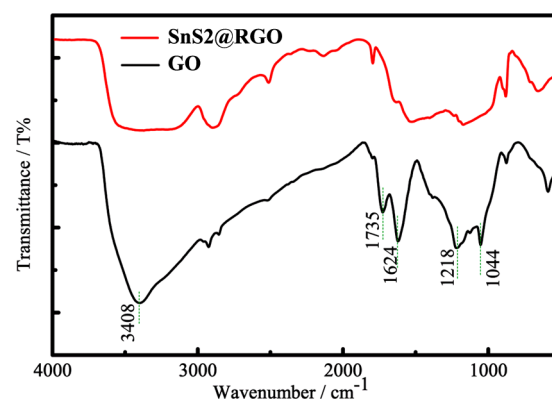

Figure 3. FT-IR spectra of as-synthesized SnS$_2$@RGO nanocomposite and GO.

GO also demonstrated the existence of C−O−C at 1218 cm^{-1}. The CO$_2$ molecules were adsorbed by bands of GO around 1044 cm^{-1} for C−O [ν(alkoxy and epoxy)].[27−29] Both C−O and O−H absorption bands were considerably decreased after reduction. The results implied that a majority of the oxygen-containing groups were reduced,[30] which was consistent with the XRD results (Figure 1). A TEM image of pure RGO is shown in Figure 4a.
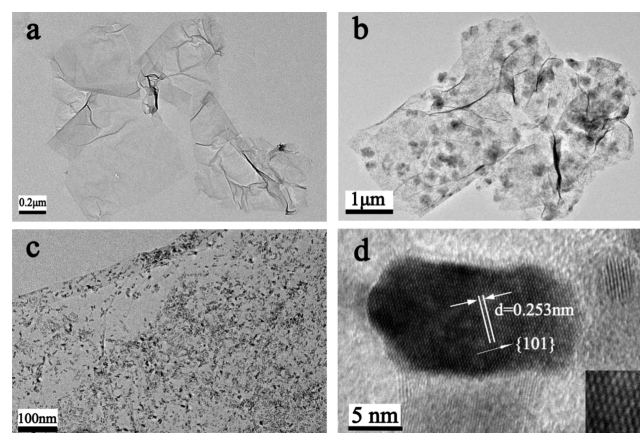

Figure 4. TEM images of as-synthesized (a) RGO and (b, c) SnS$_2$@RGO nanocomposite. (d) HRTEM image of SnS$_2$@RGO nanocomposite.

A demonstration of the synthesis of SnS$_2$@RGO nanocomposite is shown in Scheme 1. In the presence of GO substrate, SnS$_2$ nanoparticles were dispersed uniformly on the surface of RGO nanosheet with a sheet-on-sheet modalism. For one thing, SnS$_2$ nanoparticles were absorbed and restricted by RGO, and their self-assembly also been restrained. For another, the restacking of few-layer graphene layers was prevented due to the existence of SnS$_2$ nanoparticles between RGO nanosheets. Their few-layer structure may preserve their intriguing properties. Consequently, the catalytic efficiency may be enhanced due to the increased reaction sites of composite. Additionally, the photocatalyzed reaction could facilitate the absorption and transportation of photoelectrons. Because of the complementary effect of composite of RGO and SnS$_2$ nanoparticles, excellent photocatalytic performances and electrochemical properties should be exhibited.[18,31,32]

The morphologies of SnS$_2$@RGO and RGO were characterized by TEM, as shown in Figure 4. SnS$_2$ nanoparticles were commendably spread onto the RGO nanosheet with a uniform grain size of about 10−20 nm (Figure 4b,c). The high-resolution transmission electron microscopy (HRTEM) image with clear lattice fringes (Figure 4d) for SnS$_2$ nanoparticles demonstrated that as-synthesized SnS$_2$@RGO had perfect crystallinity. The lattice spacing of 0.253 nm corresponded to the d-spacing between neighbor (101) crystallographic planes of SnS$_2$ nanoparticles (d_{200} = 0.278 nm for SnS$_2$). SnS$_2$ nanoparticles aggregated before the reduction of GO. The substrates for nucleation of nanomaterials were oxygen functional groups of GO, and the well-dispersed nano-composites resulted from reciprocity between functional groups and SnS$_2$ nanoparticles during nucleation and growth.[10,33]

Electron conductivity and mass diffusion of materials could be effectively estimated from EIS. The Nyquist plot in Figure 5
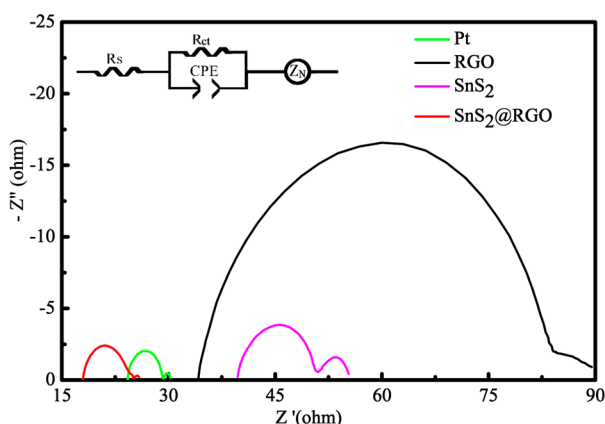

Figure 5. Nyquist plots of SnS$_2$@RGO, SnS$_2$, RGO, and Pt CEs. (Inset) Equivalent circuit diagram.

clarifies impedance characteristics of various CEs. The intercept on the horizontal axis represents the series resistance (R_s), which is mainly referred to as conductive substrate resistance and lead resistance. The first semicircle represents charge-transfer resistance (R_{ct}) at the CE/electrolyte interface and the corresponding constant phase-angle element (CPE) at the electrode−electrolyte interface. The second arc corresponds to the Nernst diffusion impedance (Z_N) between the triiodide/iodide redox couple in the electrolyte. The equivalent circuit is given in the inset of Figure 5 (detailed simulation value of equivalent circuit is listed in Table S2 in Supporting Information), which was constituted of several parts: series resistance, R_{ct} at CE/FTO layers, Z_N between the triiodide/iodide redox couple in the electrolyte, and CPE of capacitance in agreement with R_{ct}. The electron-transport mechanism was affected directly by internal impedances in DSSCs.[10] As shown in Table 1, R_{ct} values for Pt, RGO, SnS$_2$, and SnS$_2$@RGO are

24.21, 34.20, 39.73, and 17.96 Ω, respectively. The larger R_{ct} values for RGO and SnS$_2$ CEs manifested their lower catalytic competence among these CEs. Relative to RGO and SnS$_2$, SnS$_2$@RGO composite gave a much lower R_{ct} value, which reflected that the nanocomposite exhibited much higher catalytic activity than that of either component. This were because of the existence of RGO sheets, which served as the conduction pathway, and the synergistic effect between RGO and SnS$_2$.[10,31]

Tafel polarization curves were measured by recording, in symmetrical cells similar to those used in EIS measurements, the natural logarithmic current density (log J) as a function of the potential (Figure 6). The exchange current density (J_0) on
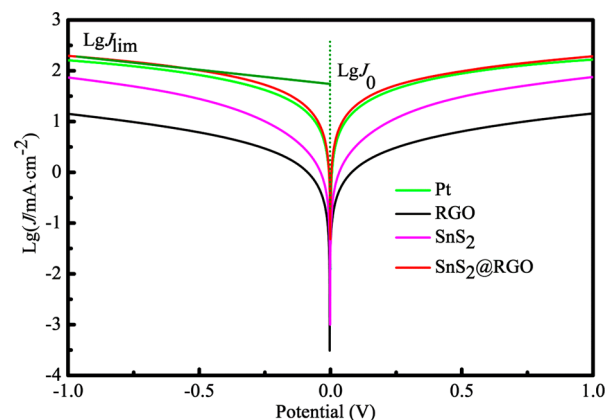

Figure 6. Tafel polarization curves of symmetrical cells fabricated various CEs.

the electrode and catalytic activity toward triiodide reduction were in proportion to the slope of the anodic or cathodic branch. The limiting diffusion current density (J_{lim}) of different electrodes corresponded to intersection of the cathodic branch with the y-axis, which can be employed to assess diffusion properties of the redox couples.[5] Table 1 gives detailed values of J_0 and J_{lim} according to eqs 1 and 2:[34]

$$J_0 = \frac{RT}{nFR_{ct}} \tag{1}$$

where R represents the gas constant, F represents the Faraday constant, T represents temperature, and n represents the number of electrons exchanged in the reaction at CE interface and the electrolyte.

$$J_{lim} = \frac{2neDCN_A}{l} \tag{2}$$

where e represents elementary charge, C represents concentration of the triiodide, D represents diffusion coefficient of the triiodide, N_A represents the Avogadro constant, and l is the

Table 1. Parameters Derived from Tafel Curves, Nyquist Plots, and DSSC Devices

	Tafel parameters		Nyquist parameters			Photovoltaic parameters			
CE	J_0 (mA·cm^{-2})	J_{lim} (mA·cm^{-2})	R_s (Ω)	R_{ct} (Ω)	Z_N (Ω)	V_{oc} (mV)	J_{sc} (mA·cm^{-2})	FF (%)	η (%)
Pt	5.05	9.11	24.21	5.08	0.95	720	14.00	67.36	6.79
RGO	1.48	3.15	34.20	50.25	5.01	661	10.8	52.29	3.73
SnS$_2$	2.99	6.51	39.73	11.24	4.36	770	13.6	53.28	5.58
SnS$_2$@RGO	5.88	9.92	17.96	7.24	0.64	718	14.80	67.02	7.12

electrode spacing. Interestingly, the results calculated from the above formula came to an agreement with the EIS values.

To further investigate the electrocatalytic properties of the samples more accurately, CV was carried out in a three-electrode system (see Figure 7a). In the previous literature,
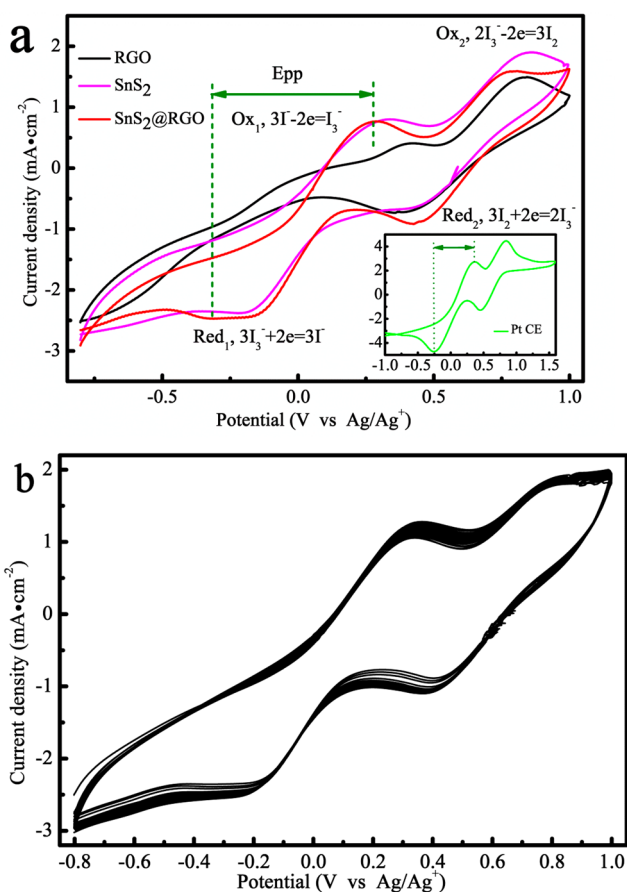

Figure 7. (a) CV curves of triiodide/iodide redox couple for RGO, SnS_2, SnS_2@RGO, and Pt electrodes. (b) Twenty-five cycles of CV curves from SnS_2@RGO nanocomposite CE at a scan rate of 50 mV·s^{-1}.

there was a typical curve with two pairs of redox peaks gained.[35] The oxidation and reduction peak on the low-potential side had a remarkable impact on the photovoltaic properties of DSSC.[36] The cathodic peak could vest in the reaction of eq 3:

$$I_3^- + 2e^- \rightarrow 3I^- \tag{3}$$

The SnS_2@RGO nanocomposite CE had a peak-to-peak splitting (E_{pp}) of 593 mV, which was very close to that of Pt CE (E_{pp} = 605 mV). This means that the reversibility and electrocatalytic activity of the oxidation−reduction reaction on SnS_2@RGO nanocomposite CE was similar to that of Pt CE. Twenty-five cycles of CV curves (Figure 7b) were used to evaluate stability of the SnS_2@RGO nanocomposite CE. No apparent decline in peak current density was observed, indicating that the SnS_2@RGO nanocomposite CEs were stable for catalyzing triiodides.[5] Therefore, SnS_2@RGO nanocomposite was expected to be a promising CE catalyst to replace the expensive Pt in DSSCs.

Figure 8 shows $J−V$ curves for all the DSSCs, and the detailed photovoltaic parameters are listed in Table 1. The DSSC utilizing SnS_2@RGO as the CE revealed a very high PCE
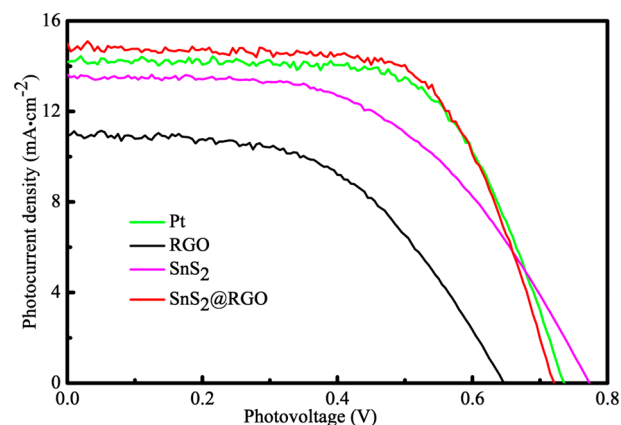

Figure 8. Photocurrent density−photovoltage ($J−V$) curves for DSSCs with different CEs.

of 7.12% by reason of the synergistic effect of SnS_2 nanoparticles on graphene, which was approximately 5% greater than the value for DSSC with Pt CE (6.79%). Under the same conditions, the DSSC with SnS_2 had subpar photovoltaic properties, which was attributed to the larger R_{ct} and lower catalytic ability,[10,37] and this was in good agreement with EIS results. Interestingly, J_{sc} was also improved observably as the cathode changed from SnS_2 or RGO to SnS_2@RGO. Considering that the photocurrent was mostly controlled by the photoanode, we discovered that it was usually similar to various cathodes as reported previously.[38] However, as photovoltaic measurements were tested under the same conditions and with the same photoanode, the increase in J_{sc} may be ascribed to the synergistic effect of RGO and SnS_2, and it may be also due to the existence of RGO nanosheets that serve as the conduction pathway. This interesting phenomenon deserves detailed investigation in the future.

4. CONCLUSIONS

In conclusion, we have successfully synthesized a nanocomposite of SnS_2 nanoparticles with reduced graphene oxide (SnS_2@RGO), which has a bright prospect as a substitute for conventional Pt catalysts used in DSSCs as counter electrode. Electrochemical tests reveal that SnS_2@RGO nanocomposite CE exhibits perfect electrocatalytic activity on reducing triiodide ions, resulting in a significant enhancement of the properties of solar cells. The nanocomposite CE achieves an impressive PCE of 7.12%, which is significantly higher than those of the SnS_2 CE (5.58%) and RGO CE (3.73%) and also comparable to the value of 6.79% obtained with a reference pure Pt CE. The fact that SnS_2@RGO nanocomposite even exceeds Pt when implemented as the CE in DSSC paves the route for the low-cost advantage of this prospective material in dye-sensitized solar cells.

■ ASSOCIATED CONTENT

Ⓢ Supporting Information

Additional text, three figures, and two tables showing PCE of DSSCs with various annealing temperatures, UV−vis absorbance spectra and optical band gap of SnS_2 and SnS_2@RGO, SEM image of SnS_2@RGO, parameters derived from DSSC devices, and simulation value of equivalent circuit. This material is available free of charge via the Internet at http://pubs.acs.org/.

■ AUTHOR INFORMATION

Corresponding Author

*Tel (+86) 0551 63861867; fax (+86) 0551 63861992; e-mail liguang1971@ahu.edu.cn or liguang64@163.com.

Notes

The authors declare no competing financial interest.

■ REFERENCES

(1) Tsoutsos, T.; Frantzeskaki, N.; Gekas, V. Environmental Impacts from the Solar Energy Technologies. *Energy Policy* **2005**, *33*, 289−296.

(2) Song, M. Y.; Chaudhari, K. N.; Park, J.; Yang, D.-S.; Kim, J. H.; Kim, M.-S.; Lim, K.; Ko, J.; Yu, J.-S. High Efficient Pt Counter Electrode Prepared by Homogeneous Deposition Method for Dye-Sensitized Solar Cell. *Appl. Energy* **2012**, *100*, 132−137.

(3) O'Regan, B.; Grätzel, M. A Low-Cost High-Efficiency Solar Cell Based on Dye-Sensitized Colloidal TiO$_2$ Films. *Nature (London)* **1991**, *353*, 737−740.

(4) Grätzel, M. Solar Energy Conversion by Dye-Sensitized Photovoltaic Cells. *Inorg. Chem.* **2005**, *44*, 6841−6851.

(5) Cai, H.; Tang, Q.; He, B.; Li, P. PtRu Nanofiber Alloy Counter Electrodes for Dye-Sensitized Solar Cells. *J. Power Sources* **2014**, *258*, 117−121.

(6) Chen, X.; Hou, Y.; Zhang, B.; Yang, X. H.; Yang, H. G. Low-Cost SnS$_x$ Counter Electrodes for Dye-Sensitized Solar Cells. *Chem. Commun.* **2013**, *49*, 5793−5795.

(7) Lee, W. J.; Ramasamy, E.; Lee, D. Y.; Song, J. S. Performance Variation of Carbon Counter Electrode Based Dye-Sensitized Solar Cell. *Sol. Energy Mater. Sol. Cells* **2008**, *92*, 814−818.

(8) Joshi, P.; Xie, Y.; Ropp, M.; Galipeau, D.; Bailey, S.; Qiao, Q. Dye-Sensitized Solar Cells Based on Low Cost Nanoscale Carbon/TiO$_2$ Composite Counter Electrode. *Energy Environ. Sci.* **2009**, *2*, 426−429.

(9) Hong, W.; Xu, Y.; Lu, G.; Li, C.; Shi, G. Transparent Graphene/PEDOT−PSS Composite Films as Counter Electrodes of Dye-Sensitized Solar Cells. *Electrochem. Commun.* **2008**, *10*, 1555−1558.

(10) Li, Z.; Gong, F.; Zhou, G.; Wang, Z.-S. NiS$_2$/Reduced Graphene Oxide Nanocomposites for Efficient Dye-Sensitized Solar Cells. *J. Phys. Chem. C* **2013**, *117*, 6561−6566.

(11) Han, S.; Hu, L.; Gao, N.; Al-Ghamdi, A. A.; Fang, X. Efficient Self-Assembly Synthesis of Uniform CdS Spherical Nanoparticles-Au Nanoparticles Hybrids with Enhanced Photoactivity. *Adv. Funct. Mater.* **2014**, *4*, 2046−2069.

(12) Novoselov, K.; Geim, A. K.; Morozov, S.; Jiang, D.; Katsnelson, M.; Grigorieva, I.; Dubonos, S.; Firsov, A. Two-Dimensional Gas of Massless Dirac Fermions in Graphene. *Nature* **2005**, *438*, 197−200.

(13) Choi, H.; Kim, H.; Hwang, S.; Han, Y.; Jeon, M. Graphene Counter Electrodes for Dye-Sensitized Solar Cells Prepared by Electrophoretic Deposition. *J. Mater. Chem.* **2011**, *21*, 7548.

(14) Lei, Y.; Song, S.; Fan, W.; Xing, Y.; Zhang, H. Facile Synthesis and Assemblies of Flowerlike SnS$_2$ and In^{3+}-Doped SnS$_2$: Hierarchical Structures and Their Enhanced Photocatalytic Property. *J. Phys. Chem. C* **2009**, *113*, 1280−1285.

(15) Ma, J. M.; Lei, D. N.; Duan, X. C.; Li, Q. H.; Wang, T. H.; Cao, A. M.; Mao, Y. H.; Zheng, W. J. Designable Fabrication of Flower-like SnS$_2$ Aggregates with Excellent Performance in Lithium-Ion Batteries. *RSC Adv.* **2012**, *2*, 3615−3617.

(16) Liu, S.; Lu, X.; Xie, J.; Cao, G.; Zhu, T.; Zhao, X. Preferential C-axis Orientation of Ultrathin SnS$_2$ Nanoplates on Graphene as High-Performance Anode for Li-Ion Batteries. *ACS Appl. Mater. Interfaces* **2013**, *5*, 1588−1595.

(17) Jiang, Z.; Wang, C.; Du, G.; Zhong, Y.; Jiang, J. In Situ Synthesis of SnS$_2$@Graphene Nanocomposites for Rechargeable Lithium Batteries. *J. Mater. Chem.* **2012**, *22*, 9494−9496.

(18) Chen, P.; Su, Y.; Liu, H.; Wang, Y. Interconnected Tin Disulfide Nanosheets Grown on Graphene for Li-Ion Storage and Photocatalytic Applications. *ACS Appl. Mater. Interfaces* **2013**, *5*, 12073−12082.

(19) Li, G.; Chen, X.; Gao, G. Bi$_2$S$_3$ Microspheres Grown on Graphene Sheets as Low-Cost Counter-Electrode Materials for Dye-Sensitized Solar Cells. *Nanoscale* **2014**, *6*, 3283−3288.

(20) Peng, L.; Hu, L.; Fang, X. Energy Harvesting for Nanostructured Self-Powered Photodetectors. *Adv. Funct. Mater.* **2014**, *24*, 2591−2610.

(21) Hirata, M.; Gotou, T.; Horiuchi, S.; Fujiwara, M.; Ohba, M. Thin-Film Particles of Graphite Oxide 1: High-Yield Synthesis and Flexibility of the Particles. *Carbon* **2004**, *42*, 2929−2937.

(22) Liu, M.; Yang, J.; Feng, S.; Zhu, H.; Zhang, J.; Li, G.; Peng, J. Composite Photoanodes of Zn$_2$SnO$_4$ Nanoparticles Modified SnO$_2$ Hierarchical Microspheres for Dye Sensitized Solar Cells. *Mater. Lett.* **2012**, *76*, 215−218.

(23) Ferrari, A. C.; Basko, D. M. Raman Spectroscopy as a Versatile Tool for Studying the Properties of Graphene. *Nat. Nanotechnol.* **2013**, *8*, 235−246.

(24) Gupta, A.; Chen, G.; Joshi, P.; Tadigadapa, S.; Eklund, P. Raman Scattering from High-Frequency Phonons in Supported N-Graphene Layer Films. *Nano Lett.* **2006**, *6*, 2667−2673.

(25) Cong, C.; Yu, T.; Sato, K.; Shang, J.; Saito, R.; Dresselhaus, G. F.; Dresselhaus, M. S. Raman Characterization of ABA- and ABC-Stacked Trilayer Graphene. *ACS Nano* **2011**, *5*, 8760−8768.

(26) Stankovich, S.; Dikin, D. A.; Piner, R. D.; Kohlhaas, K. A.; Kleinhammes, A.; Jia, Y.; Wu, Y.; Nguyen, S. T.; Ruoff, R. S. Synthesis of Graphene-Based Nanosheets via Chemical Reduction of Exfoliated Graphite Oxide. *Carbon* **2007**, *45*, 1558−1565.

(27) Nethravathi, C.; Rajamathi, M. Chemically Modified Graphene Sheets Produced by the Solvothermal Reduction of Colloidal Dispersions of Graphite Oxide. *Carbon* **2008**, *46*, 1994−1998.

(28) Szabó, T.; Berkesi, O.; Forgó, P.; Josepovits, K.; Sanakis, Y.; Petridis, D.; Dékány, I. Evolution of Surface Functional Groups in a Series of Progressively Oxidized Graphite Oxides. *Chem. Mater.* **2006**, *18*, 2740−2749.

(29) Nie, G.; Zhang, L.; Lu, X.; Bian, X.; Sun, W.; Wang, C. A One-Pot and in Situ Synthesis of CuS-Graphene Nanosheet Composites with Enhanced Peroxidase-like Catalytic Activity. *Dalton Trans.* **2013**, *42*, 14006−14013.

(30) Chen, C.; Long, M.; Xia, M.; Zhang, C.; Cai, W. Reduction of Graphene Oxide by an In-Situ Photoelectrochemical Method in a Dye-Sensitized Solar Cell Assembly. *Nanoscale Res. Lett.* **2012**, *7*, 1−5.

(31) Zhang, D. W.; Li, X. D.; Li, H. B.; Chen, S.; Sun, Z.; Yin, X. J.; Huang, S. M. Graphene-Based Counter Electrode for Dye-Sensitized Solar Cells. *Carbon* **2011**, *49*, 5382−5388.

(32) Stankovich, S.; Dikin, D. A.; Dommett, G. H.; Kohlhaas, K. M.; Zimney, E. J.; Stach, E. A.; Piner, R. D.; Nguyen, S. T.; Ruoff, R. S. Graphene-Based Composite Materials. *Nature* **2006**, *442*, 282−286.

(33) Li, Y.; Zhao, Y.; Cheng, H.; Hu, Y.; Shi, G.; Dai, L.; Qu, L. Nitrogen-Doped Graphene Quantum Dots with Oxygen-Rich Functional Groups. *J. Am. Chem. Soc.* **2011**, *134*, 15−18.

(34) Hauch, A.; Georg, A. Diffusion in the Electrolyte and Charge-Transfer Reaction at the Platinum Electrode in Dye-Sensitized Solar Cells. *Electrochim. Acta* **2001**, *46*, 3457−3466.

(35) Wu, M.; Lin, X.; Hagfeldt, A.; Ma, T. A Novel Catalyst of WO$_2$ Nanorod for the Counter Electrode of Dye-Sensitized Solar Cells. *Chem. Commun.* **2011**, *47*, 4535−4537.

(36) Wu, M.; Bai, J.; Wang, Y.; Wang, A.; Lin, X.; Wang, L.; Shen, Y.; Wang, Z.; Hagfeldt, A.; Ma, T. High-Performance Phosphide/Carbon Counter Electrode for both Iodide and Organic Redox Couples in Dye-Sensitized Solar Cells. *J. Mater. Chem.* **2012**, *22*, 11121−11127.

(37) Yen, M.-Y.; Hsiao, M.-C.; Liao, S.-H.; Liu, P.-I.; Tsai, H.-M.; Ma, C.-C. M.; Pu, N.-W.; Ger, M.-D. Preparation of Graphene/Multi-

Walled Carbon Nanotube Hybrid and Its Use as Photoanodes of Dye-Sensitized Solar Cells. *Carbon* **2011**, *49*, 3597–3606.

(38) Kavan, L.; Yum, J. H.; Gratzel, M. Graphene Nanoplatelets Outperforming Platinum as the Electrocatalyst in Co-Bipyridine-Mediated Dye-Sensitized Solar Cells. *Nano Lett.* **2011**, *11*, 5501–5506.